Master of Science Thesis in Electrical Engineering
Department of Electrical Engineering, Linköping University, 2016

# Development of a vehicle simulation model consisting of low and high frequency dynamics

**Dennis Belousov**

Master of Science Thesis in Electrical Engineering

**Development of a vehicle simulation model consisting of low and high frequency dynamics**

Dennis Belousov

LiTH-ISY-EX--16/5002--SE

Supervisor: **Mahdi Morsali**
ISY, Linköping University
**Robert Johansson**
NIRA Dynamics AB

Examiner: **Jan Åslund**
ISY, Linköping University

*Division of Vehicular Systems*
*Department of Electrical Engineering*
*Linköping University*
*SE-581 83 Linköping, Sweden*

# Sammanfattning

Eftersom fordonstester av existerande fordon är mycket tids- och resurskrävande, efterfrågas en metod för effektivare testning av säkerhetsalgoritmer i fordonsindustrin. Målet i detta exjobb är att studera och ta fram en fordonssimuleringsmodell som kan simulera önskad dynamik både i existerande och icke-existerande fordon.

Den framtagna modellen delas in i två områden: långsam dynamik och vibrationsdynamik. Dessa två områden är framtagna och validerade genom olika metoder. I den slutliga simulatorn är dessa dock avsedda att simuleras tillsammans.

Vad gäller den långsamma dynamiken rörande låga frekvenser har en tillståndsmodell för fordonets rörelse med tre tillstånd tagits fram och undersökts. Möjligheterna för parameteranpassning till modellen har studerats med hjälp av prediktionsfelsminimering.

För vibrationsmodellen som består av högra frekvenser har en linjär kvartbilsmodell i kombineration med hjuldynamik används för att estimera vägens vibrationskarakteristik. Den estimerade vägen används för att simulera fordonets beteende. De föreslagna metoderna studeras genom frekvensanalys eftersom vägen är av stokastisk natur och ej är känd deterministiskt. Hjulhastigheterna används för frekvensanalysen eftersom de är tillgängliga i höga samplingsfrekvenser.

De tillgängliga verktygen och sensorerna som används under exjobbet är begränsade till existerande fordonssensorer och GPS-signaler. Resultatet av denna begränsning studeras och diskussion förs angående dess resultat.

# Abstract

As vehicle testing on existing vehicles is both time and resource consuming, the work of testing safety algorithms on vehicle is desired to be made more efficient. Therefore the goal of this thesis is to study and develop a vehicle simulation model that can simulate desired dynamics of existing and non-existing vehicles.

The developed model consist of two areas of application: slow dynamics and vibrational dynamics. These areas are developed and validated using different methods, but as a part of the simulator, they are to be simulated together.

For the slow, low frequency, vehicle motion, a three state transient motion model is derived and examined. The possibility of parametrisation is studied and performed using prediction error minimisation.

For the vibration, high frequency model, a combination of a linear quarter car model with wheel motion is used to estimate road vibration characteristics. The modelled road is used to simulate the vehicle behaviour. The suggested methods regarding the vibration modelling and road estimation are performed using power spectral density as the road is not known determinately. Wheel speeds are used to study the power spectral densities as they are available at high sampling frequencies.

The available tools and sensors used during this thesis are limited to existing vehicle sensors and GPS signals. The effect of this limitation is studied and the results are discussed.

## Acknowledgments

I would like to thank my supervisor Robert Johansson at NIRA Dynamics for his enthusiasm and support throughout the thesis. All our meetings have helped me through parts of the thesis that I initially thought were rough. Rickard Karlsson from NIRA Dynamics has provided extra guidance of the thesis for which I am grateful. Mahdi Morsali, my supervisor from Linköping university, deserves a thanks for his oversight of my work and help with my written documents. I am also grateful to Jan Åslund for his assistance as the examiner. A final thanks is extended to all my co-workers who have shown interest in my work and have participated in discussions.

*Linköping, September 2016*
*Dennis Belousov*

# Contents

# Notation

**Parameters**

| Parameter | Meaning |
|---|---|
| $\mu_p$ | Road friction coefficient. |
| $m$ | Vehicle mass. |
| $W$ | Normal force acting on a wheel. |
| $C_{\alpha_f}$ | Cornering stiffness coefficient at the front wheel. |
| $C_{\alpha_r}$ | Cornering stiffness coefficient at the rear wheel. |
| $C_s$ | Longitudinal tire stiffness (normal force dependent). |
| $\kappa$ | Longitudinal tire stiffness. |
| $s$ | Slip, Laplace operator. |
| $\alpha$ | Road inclination. |
| $\omega$ | Wheel angular velocity. |
| $\theta$ | Frequency vector, parameter vector, vehicle rotation angle. |
| $F$ | Force. |
| $R$ | Resistance force. |
| $v$ | Vehicle velocity. |
| $V$ | Road amplitude, cost function. |
| $I_z$ | Vehicle rotational inertia. |

### Abbreviations

| Abbreviation | Meaning |
|---|---|
| CAN | Controller area network. |
| FL | Front left (wheel). |
| FR | Front right (wheel). |
| GPS | Global positioning system. |
| ISO | International organisation of standardization. |
| LTI | Linear, time-invariant (system). |
| PEM | Prediction error minimisation. |
| PSD | Power spectral density. |
| RL | Rear left (wheel). |
| RPM | Revolutions per minute. |
| RR | Rear right (wheel). |

# 1 Introduction

## 1.1 Background

In order to evaluate any new technology, it has to go through rigorous testing, both during development and the final performance verification. In the automotive industry this is usually done in field testing of existing cars or prototypes. The obvious advantage is, of course, that the vehicle behaviour is examined during real circumstances. There are, however, several downsides of field testing as well. It is expensive, as the physical vehicle has to be available as well as resources like drivers and fuel are used; the reproducibility is low due to changing weather and traffic conditions; the collection of large amounts of data and test cases take a long time and the vehicles can rarely be pushed to their capability limit due to safety concerns.

This Master's thesis is performed at NIRA Dynamics AB that specialize in automotive software solutions for monitoring wheel and road states. Their main idea is to use signal processing and sensor fusion to estimate these states without the addition of extra hardware, *i.e.* sensors. The main product of NIRA Dynamics AB is a tire pressure monitoring system.

With the background of the limitations of field testing, this Master's thesis focuses on examining the possibilities of a simulator that can generate data from test cases like tire pressure drops on various road surfaces. As the road and wheel states and properties are tightly connected, the modelling of this connection is the main focus.

## 1.2 Goal and methodology

This Master's thesis goal is to study the characteristics of the vehicle when it is excited by the road and driver inputs in order to implement these characteris-

tics into a simulator. As the purpose of the final simulator is to simulate sensor values, the dynamics between the inputs and the measured states are to be modelled. The vehicle motion dynamics are studied and validated using prediction error minimisation, see Section 2.3, as several input and output signals are measured. Regarding the road model, it is studied via its power spectral density, see Section 2.2, as it is of stochastic nature and cannot be measured determinately in this thesis.

## 1.3 Related research

A lot of research has been done on both vehicle, tire and road modelling. While the vehicle dynamics modelling is more straightforward than the tire and road modelling, and mainly varies in complexity, there are many different attempted approaches in describing the road.

### 1.3.1 Vehicle modelling

General models of various complexity can be found in most vehicle dynamics books. In Wong [25], one and two track vehicle models consisting of one to three degrees of freedom are covered. The linear quarter car model and its resonance frequencies are studied for various parameters. Pitch and roll behaviour of a vehicle is covered as well.

A lot of work has been done on vehicles of various complexity and degrees of freedom. Vandi et al. [23] for instance, develops a 14-degree of freedom vehicle model that is to be used for simulation. It was desired to simulate individual torques and loads on each wheel for high performance prediction. The developed model was compared to commercial software and good correspondence was established.

Saglam and Unlusor [17], on the other hand, develop a 3-degree of freedom vehicle model in order to compare it to commercial software. Their results found that even simple model could stand up to more advanced multi-body models. This is in agreement with the conclusions of Allen and Rosenthal [1] that compare simple and complex vehicle models. It is found that for regular driving, simple models are sufficient. However, as soon as the driving nears the vehicle dynamics capability limits, more complex models are required.

### 1.3.2 Road property dependencies

In order to fully describe a road, several properties has to be accounted for. Many of these road properties are, however, not simply dependent on the road, but also on the tire and to some extent the vehicle. Friction, which is a property of the two materials in contact, is not the only co-property. As it is found in Soliman [19] and Hoever and Kropp [4], the vehicle rolling resistance in the contact patch is dependent on the road roughness. It is even found that the road roughness and the tire-road friction are dependent on one another as concluded in Rath et al. [16].

Since the road friction depends on the vertical tire load, which in turn depends on the road roughness, the road profile and road friction are not mutually independent. In Rath et al. [16] both these are estimated simultaneously as a non-linear Lipschitz observer and a modified super-twisting algorithm observer is developed. In their paper, the estimations were successful, even in the presence of disturbances.

In Karlsson et al. [7] the effect of the road surface on the rolling resistance is examined. A model depending on mean profile depth and the International Roughness Index is adapted to the measurements performed. It is found that out of three attempted methods, only the coast down method provides any information on the effect of the road unevenness on the rolling resistance.

In Türkay and Akcay [21] the effect of random road excitations on a quarter-car is examined. The road disturbances were modelled as white noise velocity input and coloured noise taken as the output from a linear shape filter. The analysis finds that best fit was established for high-order shape filters. The integrated white noise road disturbance had better fit than a second-order shape filter, but was only reliable at lower speeds.

In Sandu et al. [18] stochastic modelling of off-road terrain was used for simulations of vehicle behaviour. In the paper, off-road properties like the pressure-sinkage relation in the contact patch are taken into account. The authors concluded that it was possible to simulate the terrain profile using stochastic modelling.

### 1.3.3 Road analysis methods

There are several methods of measuring road roughness: IRI, roughness standard deviation, power spectral density (PSD), plane index and root mean square of the vertical acceleration, to name a few.

Jiang et al. [5] uses Inverse Fast Fourier Transform (IFFT) to model the road roughness. According to the authors, the IFFT method has a better degree of fitting than other roughness modelling methods like harmonic superposition, AR/AR method, Pseudo-white noise method, the filtered Poisson method, wavelet analysis, fractal reconstruction and the neural network method that was tested.

Hesami and McManus [3] compare the PSD approach to a wavelet approach as determining the roughness using signal processing. In the study, it is found that there exists correlation between the attempted approaches and the already established measures like IRI. It was also concluded that wavelet analysis outperformed PSD, especially when it came to local analysis like road variations, cracks and potholes.

Quan et al. [15] perform an analysis of the road roughness based on multi-fractal theory. Their conclusions are that multi-fractal theory is complementary to for instance IRI, with the extra detail of being able to specify local road characteristics as well.

Wang et al. [24] use the FFT on the vertical accelerometers. The proposed method uses a quarter car model and is independent of other vehicle parameters as well as the vehicle speed. According to the authors, the proposed method is

comparable to other methods.

Lambeth et al. [9] develops a continuous-state Markov chain to model the road profile with few parameters. The approach is stochastic, which allows variations in the simulations with the same road characteristics. In the article the conditional transition probabilities between the states are represented. In the study, measurements of the height of the road profile was known. Possible future improvements that are mentioned are in the sliding window that is used to estimate the model parameters, where improved windows could yield better estimates.

In Kawale and Ferris [8] an autoregressive model is adapted to measured data to model the road profile. A terrain measurement system is used to scan the road using lasers.

Yokohama and Randall [26] studied the roughness of the road's performance on rubber tires. This was done on the level of the surfaces random height distribution, modelled as a Gaussian and non-Gaussian surface using Finite Element Analysis (FEA). An effect of the roughness on the friction was observed, as on asphalt more stick-slip behaviour was observed for various normal pressures on the wheel. The results were, however, not verified using experimental data.

### 1.3.4 Tire models

Pacejka [14] covers several tire models, like the brush model, the thread simulation model, the similarity model, the Magic Formula Model (MFM) and the stretched string model. Both steady state and transient behaviour is covered.

Li et al. [10] compare and evaluate many tire models and categorize them according to their application area: handling analysis, ride comfort analysis or durability analysis. According to the paper, the performance predictions of handling analysis needs to be improved, as well as the desire for a more efficient way to identify the tire model parameters.

Li and Sandu [11] develop a modelling approach based on Friction Ellipse Model (FEM) and MFM to predict the tire response during the stochastic uncertainties of tire parameters. The study concluded that the developed models were able to predict the tire behaviour during steady-state cornering while key tire parameters varied about a certain value with a uniform distribution.

### 1.3.5 General modelling and simulation

Ljung and Glad [12] contains theory on various models and model structures like autoregressive moving average models, physical models, bond graphs, differential algebraic equation models, system and parameter estimation methods along with correlation and spectral analysis.

Suresh and Gilmore [20] brings up discussions about the needed complexity of vehicle models to be used for simulation. Discussions regarding the subjects of model development, parameter estimation and analysis of the simulation validity. These are all important to consider before, during and after modelling.

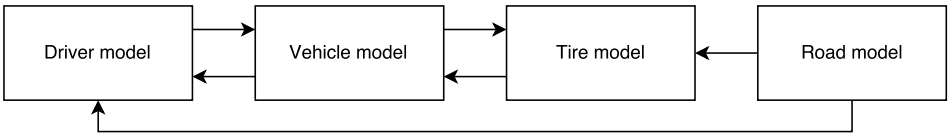


***(a)*** *Illustrating the end usage of of the simulator.*

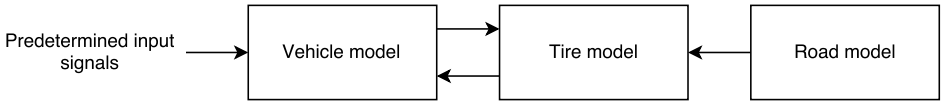


***(b)*** *Illustration of the modules in the scope of the thesis.*

***Figure 1.1:*** *Flowcharts of the models in the simulator.*

## 1.4 Project scope and limitations

Since the development of a full fledged simulator is a long and complicated process, the scope of this thesis has to be specified. Figure 1.1 shows the set-up of the expected simulator flow as well as the modules that this thesis is limited to. Any internal dependencies like the engine and drive-line are not studied in this thesis.

The application area of the model is also limited to on-road conditions as well as non-extreme driving. The reasons for this is to be able to focus the thesis more deeply on the usual conditions. Another reason for the more casual driving is that the collected data is no longer reliable if some form of active control engages as there is no information on the magnitude of its effect on the vehicle.

## 1.5 Test vehicle and equipment

The test vehicle used to collect data is a Fiat 356 sedan. It is front wheel driven and has a independent type McPerson suspension on the front axle and a semi-independent spring suspension on the rear axle. It is also significantly heavier in the front than in the back.

The data available throughout this thesis is limited to the data sent over the controller area network (CAN) bus and an external global positioning system (GPS) signal. This means that the available sensors are solely those already provided in the vehicle by the car manufacturer. The full extent of the most relevant signals are shown in Table 1.1.

***Table 1.1:*** *Available signals used for modelling.*

| Signal | Sampling frequency (Hz) | Note |
|---|---|---|
| Individual wheel speeds | 120 | Using cog tics |
| Engine torque | 10 | Modeled signal from the vehicle manufacturer |
| Engine RPM | 10 | |
| Steering wheel angle | 10 | |
| Yaw rate | 10 | |
| Longitudinal acceleration | 10 | |
| Lateral acceleration | 10 | |
| Engine speed | 10 | |
| GPS | | External measurement |

# 2

# Modelling and signal theory

## 2.1 Introduction

The theory behind the two main methods used for either part of system modelling and descriptions are detailed in this chapter. The power spectral density describes the frequency content in a signal and will be used as a tool in the estimation and modelling of the road among other related signals. Prediction error minimisation is one of several methods of system identification. This method is commonly used and will be utilized in for parameter estimation of the developed vehicle models.

## 2.2 Power spectral density

The power spectral density is a measurement of the signal power component at each frequency. The study of a signal frequencies can give other information than only its time dependent version. This is useful in the study of vibrations. As opposed to energy spectral density useful for signals of finite energy where the Fourier transform exist, the PSD is used for signals of infinite energy, like, for instance, stochastic processes.

The power of a signal $x(t)$ is given by the time average

$$P = \lim_{T\to\infty} \frac{1}{2T} \int_{-T}^{T} x(t)^2 \, \mathrm{d}t. \tag{2.1}$$

Since for many signals the Fourier transform does not exist, a truncated Fourier

transform

$$x_T(\omega) = \frac{1}{\sqrt{T}} \int_0^T x(t) e^{-i\omega t} \, \mathrm{d}t \tag{2.2}$$

where $i$ is the imaginary number, $\omega$ is the phase, $t$ is time and $T$ is the truncation limit, is used. The PSD can then be defined as the expected value of the truncated Fourier transform squared

$$\Phi(\omega) = E[|x_T(\omega)^2|] \tag{2.3}$$

where $E[\,\cdot\,]$ denotes the expected value.

### 2.2.1 Estimation of power spectral densities

When calculating the raw PSD of a sampled signal the result is usually noisy and it may be difficult to distinguish system dynamics from noise. Smoothing and averaging are two methods to improve the estimated PSD.

#### Averaging

The estimated PSD using averaged periodograms decrease the variance of the estimate. This is performed by splitting the data $x(t)$ into $K$ sections. The PSD is calculated for each section and the resulting periodograms are averaged. The average PSD then becomes

$$\hat{R}[\theta] = \frac{1}{K} \sum_{k=1}^{K} \hat{R}_k[\theta] \tag{2.4}$$

where $\hat{R}_k[\theta]$ is the $k$'th estimate and $\theta$ is the frequency. As the data used for the calculation of each PSD is decreased by a factor $K$, the resolution of the calculated and therefore also the averaged PSD have their frequency resolution decreased by the same factor.

#### Smoothing

A method used to smooth the PSD is by multiplication of the data by a window $w(t)$. This multiplication transforms into a periodical convolution with a window in the time domain.

There are a large number of different windows that can be used: the rectangular window, triangular window, Hanning window, Hamming window and Blackman window to name a few. The transformed windows all have a similar look of one main lobe and several smaller side lobes. The main lobe width determines to the amount of smoothing while the side lobes give rise to leakage of other frequencies into a given frequency. The windows have slightly different properties when it comes to the level of trade off between smoothing, detail and leakage. Whatever is desired is dependent on the data and a suitable level of trade-off in smoothing and detail.

Equivalent derivations and explanations of the PSD theory stemming from signal theory using the autocorrelation function can be studied further in Olofsson [13].

## 2.3 Prediction error minimisation

One method of parameter estimation is the minimisation of a prediction error of a model using set parameters compared to measured data [12]. This method is useful when the measured system outputs can be predicted using a model with the same, known inputs. The prediction error is measured using a cost function

$$V_N(\theta) = \frac{1}{N}\sum_{k=1}^{N} L(e(t_k)), \tag{2.5}$$

where the minimising criterion for multivariate systems is

$$L(e(t_k)) = e^T \Lambda^{-1} e \tag{2.6}$$

using a positive semi-definite $p \times p$ matrix $\Lambda$ that weights together the relative importance of the error. The error is is given by

$$e(t_k) = y(t_k) - \hat{y}(t_k|\theta) \tag{2.7}$$

where $y(t_k)$ is the measured system output and $\hat{y}(t_k|\theta)$ is the predicted measurement the output from the model using the parameters in $\theta$ at time $t_k$, The estimated optimal choice of parameters is given by the vector

$$\hat{\theta} = \arg_\theta \min V_N(\theta). \tag{2.8}$$

A well used tool for grey box prediction error minimisation is the `pem` function in Matlab included in the system identification toolbox.

# 3

# Methodology

## 3.1 Model set-up

The models specified to be developed are the vehicle, tire and road model. In this thesis, the models are studied in two different areas: slow dynamics and vibrations. The slow dynamics are the general low frequency movements of the vehicle, dependent on the driver inputs, road inclination and weather conditions. The general case is transient motion with where the desired model complexity governs the amount of freedom degrees. A special case of this is purely longitudinal motion which will be studied first. This is in order to have the possibility to separate the parameter estimation and so that different sources of errors are not mixed.

The vibration dynamics are mainly excited by high frequency sources. The road is one of these excitation sources and is studied together with the vehicle components mainly affected by the road. This means the road will be modelled closely to the vehicle components wheel and suspension system. An important reason for this set-up is that within the scope of this thesis, the road as an input is an unknown signal. Therefore conventional modelling and validation methods where the system is simulated using known inputs cannot be used for the vibration dynamics. Instead, the vibration dynamics will be studied in a stochastic manner using PSD. The engine is also one of the major vibration sources as it operates at high frequencies, but this dependence is not studied in this thesis.

## 3.2 Vehicle dynamics

The slow dynamics of the vehicle is divided into two application areas. The first is the special case of pure longitudinal motion where the velocity is varying and there is no steering wheel output. This is later expanded into transient motion

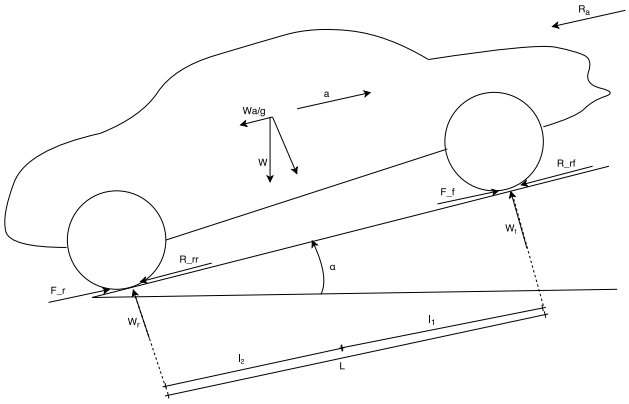


***Figure 3.1:*** *Forces acting on a vehicle during longitudinal motion.*

where cornering is included as the steering wheel angle is time varying. This set-up is made in order for system identification of the vehicle to be approached in two steps. Firstly, the longitudinal motion is studied in order to determine some parameters. Afterwards, other parameters are estimated using the transient model. If all parameters would be to be estimated from the transient model, further assumptions and simplifications regarding the road inclination would have been necessary.

### 3.2.1 Longitudinal motion

The forces acting on a vehicle during longitudinal motion are depicted in Figure 3.1. This gives the vehicle motion equation

$$m\frac{\mathrm{d}v}{\mathrm{d}t} = F_x - R_a - R_g - R_r. \tag{3.1}$$

In this case the vehicle velocity $v = v_x$ is known as it is derived from the wheel speeds of the non-driving wheels, $F_x$ is the resulting traction force in the contact patch, $R_a$ is the air resistance (drag included) and $R_r$ is the rolling resistance. The subscript $x$ denotes the longitudinal direction.

Moment equality of the forces and torques acting on a driving wheel in Figure 3.2 gives

$$I_w\dot{\omega} = T_w - T_r - rF_x + rR_r \tag{3.2}$$

where $T_w$ is the torque acting on the axle, $T_r$ is any torque resistance (neglected as it is unknown and considerably smaller than $T_w$) and $I_w$ is the wheel inertia. The wheel torque is expressed as

$$T_w = T_e\eta \tag{3.3}$$

where the torque provided by the engine is $T_e$ and $\eta$ is the gear ratio. The torque is usually modelled by the car manufacturer, and the estimated torque is sent

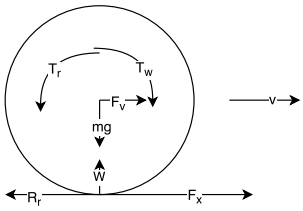


***Figure 3.2:*** *Forces and torques acting on a driving wheel.*

over the CAN bus. It is therefore considered a known signal as the estimated torques are often accurate. The gear ratio $\eta$ is defined as the ratio of the angular velocity of the engine to the one of the driving wheels according to

$$\eta = \frac{4\pi\zeta}{60(\omega_{FL} + \omega_{FR})} \tag{3.4}$$

where $\zeta$ is the engine RPM.

The rolling resistance is modelled empirically as $R_r = (a + bv^2)W$ as in Wong [25]. The air resistance is modelled according to

$$R_a = \rho A_f C_d v_x^2/2 \tag{3.5}$$

where $\rho$ is the air density, $A_f$ is the vehicle frontal area and $C_d$ is drag coefficient dependent on the vehicle shape [25].

As the value measured by the longitudinal accelerometer during longitudinal driving is

$$a_x = \sin(\alpha)g + \dot{v}_x + e \tag{3.6}$$

where $\alpha$ is the road inclination and $e$ is the sensor offset and noise. A virtual sensor estimate of the the gravitational resistance could then be expressed as

$$R_g = m(a_x - \dot{v}_x) \tag{3.7}$$

where the gravitational resistance (and noise) is the only remaining component in $R_g$.

Substituting $F_x$ from (3.2) into (3.1) with the conversion of angular wheel speed to linear vehicle speed $v = \omega r$ as well as (3.3) and (3.5) to expand the products the differential equation governing the vehicle velocity becomes

$$\underbrace{\left(m + \frac{I_w}{r^2}\right)}_{\tilde{m}}\dot{v} = \frac{T_e\eta}{r} - \underbrace{\left(\frac{\rho A_f C_d}{2} + bW\right)}_{A_{\text{air}}}v^2 - R_g + aW. \tag{3.8}$$

In this equation, $v$ is the state, $R_g$, $T_e$ and $\eta$ are inputs and the rest are parameters. The equivalent dynamics of Figure 3.2 for the non-driving wheels have been neglected. This is due to unknown size of any internal resistance that would give rise to a torque on the rear wheels.

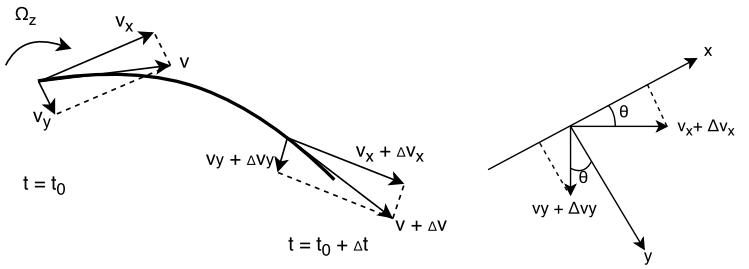


***(a)*** *Velocity components of a vehicle in during transient motion.*

***(b)*** *Illustration of the vehicle component angels after a small rotation.*

***Figure 3.3:*** *Illustration of the one-track vehicle model.*

### 3.2.2 Transient motion

The general case of vehicle motion is when the vehicle is turning and not necessarily is in steady-state. As the vehicle is turning, there is an additional velocity component in the change of the vehicle longitudinal and lateral velocity, $v_x$ and $v_y$. The velocity change during vehicle rotation in a short time $\Delta t$ can be seen in Figure 3.3a and the corresponding changes in the velocities are illustrated in Figure 3.3b as the vehicle has rotated an angle $\theta$ considered very small ($\theta = \Delta\theta$), during a short time $\Delta t$. The change of velocity in the longitudinal direction is

$$(v_x + \Delta v_x)\cos\Delta\theta - v_x - (v_y + \Delta v_y)\sin\Delta\theta \approx \Delta v_x - v_y\Delta\theta \tag{3.9}$$

where the small angle approximation is used. In the limit of $\Delta t \to 0$ the actual acceleration becomes

$$a_x = \frac{\mathrm{d}v_x}{\mathrm{d}t} - v_y\frac{\mathrm{d}\theta}{\mathrm{d}t} = \dot{v}_x - v_y\Omega_z. \tag{3.10}$$

An extension of the longitudinal model to transient motion is modelled using the one-track model illustrated in Figure 3.4 [25]. This model consists of three states: the longitudinal velocity $v_x$, the lateral velocity $v_y$ and yaw rate $\Omega_z$. The left and right hand side wheels are combined which reduces the degrees of freedom as roll is neglected. As in the longitudinal case, pitch is also not modelled. Even though roll and pitch affects the load transfers on the tires and thereby has an impact on the traction of individual wheels, these effects are attempted to be minimised as the driving style is made non-extreme. In this scenario other factors like air resistance $R_a$, rolling resistance $R_r$, gravitational acceleration $R_g$ are still greatly acting on the vehicle and are thus modelled.

The vehicle transient motion can be described using the differential equations

$$m\left(\frac{\mathrm{d}v_x}{\mathrm{d}t} - v_y\Omega_z\right) = F_{xf}\cos\delta_f + F_{xr} - F_{yf}\sin\delta_f - R_a - R_g - R_r \tag{3.11a}$$

$$m\left(\frac{\mathrm{d}v_y}{\mathrm{d}t} + v_x\Omega_z\right) = F_{yr} + F_{yf}\cos\delta_f + F_{xf}\sin\delta_f \tag{3.11b}$$

$$I_z\frac{\mathrm{d}\Omega_z}{\mathrm{d}t} = l_1F_{yf}\cos\delta_f - l_2F_{yr} + l_1F_{xf}\sin\delta_f \tag{3.11c}$$

which are derived from the illustrations in Figure 3.4. New lateral forces for the front and rear wheels in the contact patch

$$F_{yf} = 2C_{\alpha_f}\alpha_f \tag{3.12}$$

$$F_{yr} = 2C_{\alpha_r}\alpha_r \tag{3.13}$$

are modelled linearly in regards to the respective drift angle $\alpha$ via the coefficient $C_\alpha$.

According to Figure 3.4b the drift angles $\alpha_{f,r}$ can be expressed according to

$$\alpha_f = \delta_f - \frac{l_1\Omega_z + v_y}{v_x} \tag{3.14}$$

$$\alpha_r = \frac{l_2\Omega_z - v_y}{v_x}. \tag{3.15}$$

Assuming a linear output from the steering wheel to the front wheels, which generally is the case for non-luxury vehicles, the wheel angle is expressed $\delta_f =$

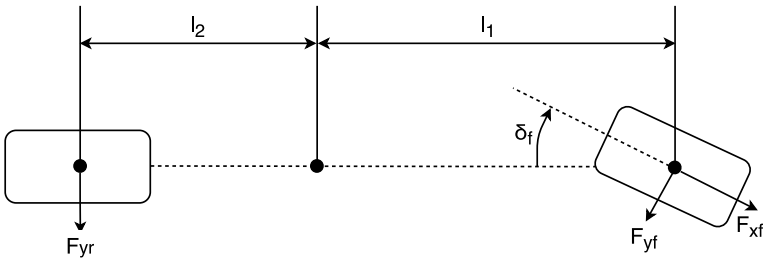


***(a)*** *Forces and dimensions.*

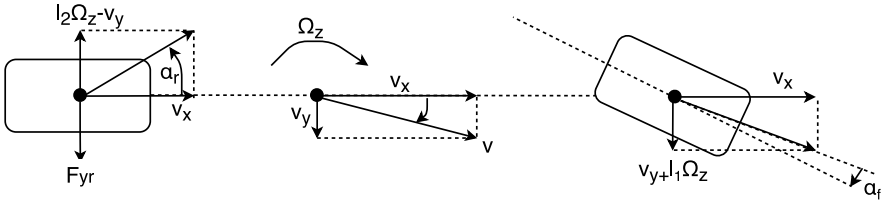


***(b)*** *Velocities and rotations.*

***Figure 3.4:*** *Illustration of the one-track vehicle model.*

$C_{cw}\delta_{sw}$ where the proportionality constant $C_{cw}$ easily can be measured and the steering wheel angle $\delta_{sw}$ is a known input.

The following approximations were made:

- The vehicle is modelled as a one-track.
- The resistances acting on the vehicle only affects the longitudinal dynamics.
- The vehicle motion is kept non-extreme.

The parameter estimation method used is the prediction error minimisation covered in Section 2.3 using the Matlab function `pem`.

The measured states are $v_x$ via the non-driving wheels and $\Omega_z$ using the gyroscope. To know $v_y$ some form of direct measurement like an optical speed sensor or indirect estimations like in Hammarling [2] are needed. These alternate methods are either not available or feasible within the limitations of this thesis, which means that $v_y$ is unknown.

A limitation imposed on the system identification is that the effect of gravity and angular acceleration cannot be distinguished in the accelerometer data. The value measured by the longitudinal accelerometer is (3.10) with the gravitational component $a_g$ included according to

$$a_x = \dot{v}_x - v_y\Omega_z + a_g. \tag{3.16}$$

Since both $v_y$ and $a_g$ are unknown $a_g$ cannot be estimated like in the longitudinal case.

## 3.3 Road descriptions

A method of describing the road roughness is through the road profile frequency energies, *i.e.* the road PSD. The road PSD can be described according to the power-law

$$S = C_{sp}\Omega^{-N} \tag{3.17}$$

for various values of the constants $C_{sp}$ and $N$. $\Omega$ is the spatial road frequency expressed in cycles per meter. The few different road PSD are shown in Figure 3.5 using road parameters, $C_{sp}$ and $N$, detailed in Wong [25]. The spatial frequency is connected to the temporal frequency $f$ via the road sampling speed (in this case the vehicle velocity $v$) according to

$$f = \Omega v. \tag{3.18}$$

Even though the road is experienced at different frequencies for various vehicle velocities, the power of each road frequency element remains the same. It is merely shifted in location according to (3.18). As the power content of each frequency component remains the same,

$$S_g(f)\,\mathrm{d}f = S_g(\Omega)\,\mathrm{d}\Omega \tag{3.19}$$

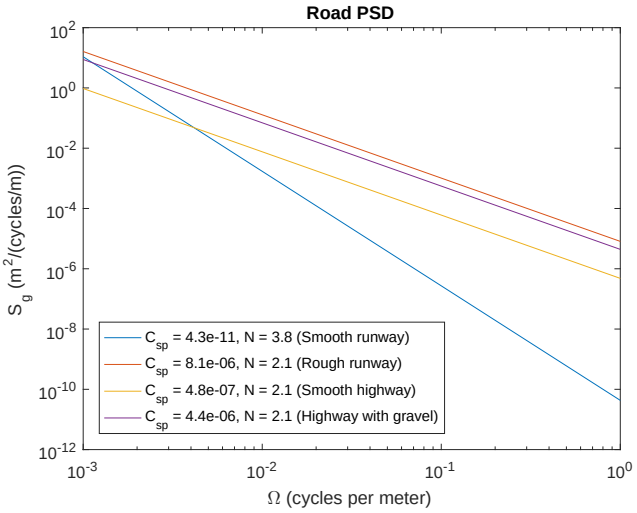


***Figure 3.5:*** *The theoretical road roughness PSD $S_g$ for a few different roads.*

holds. This is equivalent to the mean-square of the road profile, the integrals of (3.19), remaining constant. Using (3.18) for a infinitesimal portion gives

$$S_g(f) = \frac{S_g(\Omega)}{v}. \tag{3.20}$$

A roughness classification based on the PSD has been set by ISO. The road classes are defined according to a split power-law

$$S(n) = \begin{cases} C_{sp,l}\Omega^{-N_l}, & \Omega \leq \Omega_0 \\ C_{sp,h}\Omega^{-N_h}, & \Omega > \Omega_0 \end{cases} \tag{3.21}$$

which, in log-log scale, is a continuous curve consisting of two lines with usually different slopes connected at $\Omega_0 = 1/(2\pi)$. The parameter $N_l$ (the slope in log-log scale) for low frequencies is usually higher than $N_h$ for high frequencies.

### 3.3.1 Simplified road disturbance

The road profile characteristics can be measured using its PSD as illustrated in Figure 3.5. This can be approximated as

$$S_g(\Omega) = C_{sp}\Omega^{-2} \tag{3.22}$$

as $N$ usually is close to 2. This allows simulation of the road profile as done in Türkay and Akcay [21].

Using $S_g(f) = S_g(\Omega)/v$ to convert from spatial to temporal frequencies and $\omega = 2\pi f$ to convert to angular frequencies the PSD can be described and spectral factorized according to

$$S_g(\Omega) = vS_g(f) = vC_{sp}\frac{(2\pi)^2}{\omega^2} = \frac{2\pi\sqrt{vC_{sp}}}{i\omega}\frac{2\pi\sqrt{vC_{sp}}}{-i\omega}. \tag{3.23}$$

This gives the transfer function

$$G(s) = \frac{2\pi\sqrt{vC_{sp}}}{s} \tag{3.24}$$

using the Laplace variable $s = i\omega$, with which the Fourier transform of the road profile $V(s) = G(s)W(s)$ transformed to the time domain gives

$$\frac{\mathrm{d}V}{\mathrm{d}t} = 2\pi\sqrt{vC_{sp}}w(t) \tag{3.25}$$

where $w(t)$ is white noise with $E(w) = 0$ and $Var(w) = 1$. This means that a road profile of PSD in (3.22) can be simulated using white noise as velocity input of the road.

## 3.4 The road profile effect on wheel speeds

The effect of the road profile on the wheel speeds will be studied in this section.

### 3.4.1 Linear quarter car modelling

A quarter car model is excited by the road profile as depicted in Figure 3.6. The road profile enters as $V$ modeled as a point contact with the tire. The tire is assumed to always be in contact with the road. The tire damping is neglected as it is low.

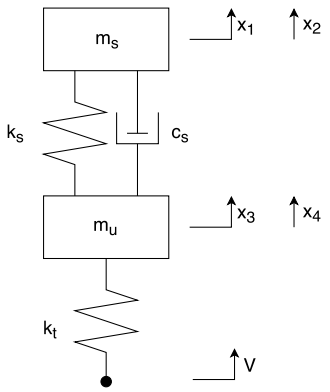


***Figure 3.6:*** *Quarter car model.*

The states in the quarter car model are defined as follows:

$$\begin{cases} x_1: & \text{Distance of the sprung mass from its equilibrium point} \\ x_2: & \text{Velocity of the sprung mass} \\ x_3: & \text{Distance of the unsprung mass from its equilibrium point} \\ x_4: & \text{Velocity of the unsprung mass} \end{cases} \tag{3.26}$$

These states make up the state space vector

$$X = \begin{pmatrix} x_1 & x_2 & x_3 & x_4 \end{pmatrix}^T. \tag{3.27}$$

The quarter car modelled is assumed linear. Even if the actual system is not linear, this model is expected to be able to describe the simpler, first order effects of the road-vehicle interaction. Vehicles often do have non-linear dampers. These dampers are explored in Section 3.4.2. Newtons second law describes the dynamics of the system as

$$m_s\ddot{x}_1 = k_s(x_3 - x_1) + c_s(\dot{x}_3 - \dot{x}_1) \tag{3.28a}$$

$$m_u\ddot{x}_2 = k_s(x_1 - x_3) + c_s(\dot{x}_1 - \dot{x}_3) + k_t(V - x_3). \tag{3.28b}$$

This model is linear and therefore the proportionality constant $k$ for a spring is the quotient of spring force to spring elongation, and the proportionality constant $c$ is the quotient of the damper force to the damper velocity. The dynamic equations are rewritten on the linear state space form $\dot{X} = AX + BV$, see Appendix A, where the matrices are defined as

$$A = \begin{pmatrix} 0 & 1 & 0 & 0 \\ -k_s/m_s & -c_s/m_s & k_s/m_s & c_s/m_s \\ 0 & 0 & 0 & 1 \\ k_s/m_u & c_s/m_u & (-k_s - k_t)/m_u & -c_s/m_u \end{pmatrix} \tag{3.29a}$$

and

$$B = \begin{pmatrix} 0 \\ 0 \\ 0 \\ k_t/m_u \end{pmatrix} \tag{3.29b}$$

where $V$ is the noise with the PSD $S_g(\Omega) = C_{sp}\Omega^{-N}/v$ described in Section 3.3.

### 3.4.2 Non-linear vehicle dampers

For the linear quarter car model, all components and dynamics were assumed linear. This is a reasonable assumption for several components. The major non-linearity, however, is in the vehicle dampers. The general damping characteristic of a vehicle can be seen in Figure 3.7.

One non-linearity is that the effective damping coefficient is lowered for velocities above the split point. This is as damping should be decreased for high frequencies in order to minimise the transmissibility of disturbances. Equivalently, for lower frequencies/velocities damping should be large in order to minimise the transmissibility of disturbances.

The second non-linearity is the lower damping for positive velocities. This is because higher damping is not necessary during compression as additional energy gets stored in the spring. The spring will naturally resist any further compression. This is not the case during negative velocities, where as the effective damping is increased.

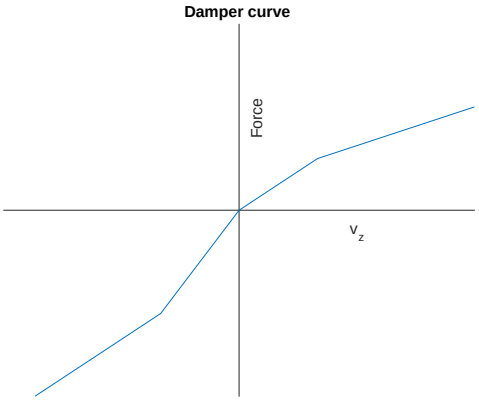


***Figure 3.7:*** *General damper characteristics in a vehicle shown as damper force against compression velocity.*

### 3.4.3 Wheel speed modelling

The normal force on the tire is

$$W = k_t(V - x_3) + N \tag{3.30}$$

where $V - x_3$ is the tire compression from its equilibrium point and N is the normal force in the equilibrium.

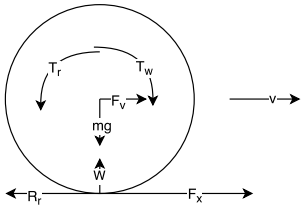


***Figure 3.8:*** *Forces and torques acting on a driving wheel.*

According to the forces and torques acting on a driving wheel as illustrated in Figure 3.8, using moment equality gives

$$I_w\dot{\omega} = T_w - T_r - rF_x + rR_r \tag{3.31}$$

where $T_w$ is the torque resulting from the engine acting on the wheel, $T_r$ is a resistance torque due to friction losses, $r$ is the wheel radius, $F_x$ is the resulting traction force, $I_w$ is the wheel inertia and $\omega$ is the wheel angular velocity.

Whenever these forces and torques act upon a wheel the wheel starts to skid. This effect, when there is a discrepancy between the wheels linear velocity and its angular velocity converted to linear velocity, is called slip $s$. The definition of slip is

$$s = \frac{\omega r - v}{v} \tag{3.32}$$

where $r$ is the wheel rolling radius and $v$ the linear velocity.

The wheel forces in the contact patch are combined and expressed as a function of slip $s$

$$F_x - R_r = C_s s = W\kappa s \tag{3.33}$$

where $C_s$ is the longitudinal tire stiffness dependent on the normal force $W$ and $\kappa$ is the longitudinal tire stiffness not dependent on the normal force. In reality the slip results from the torque acting on the wheel and the dynamics in the contact patch, but this relation can equivalently be used to express the torque from a known slip which can be calculated in alternate ways. The torques are combined

$$T = T_w - T_r \tag{3.34}$$

as $T_r$ is unknown, and in the case of the engine torque being estimated by the car manufacturer on the driving wheels, $T_r$ is either included or neglected as it is significantly lower than $T_w$. Using the definition of slip (3.32) and (3.30) in (3.31) gives the differential equation

$$\begin{aligned} I_w\dot{\omega} =& T - r(k_t(V - x_3) + N)\kappa\left(\frac{\omega r}{v} - 1\right) \\ =& T - \frac{r\kappa k_t}{v}(\epsilon + V - x_3)(\omega r - v) \end{aligned} \tag{3.35}$$

where $\epsilon = N/k_t$. The effective wheel rolling radius and the traction force lever are assumed to be the same $r$ and also constant, even though there is a slight dependence on the tire compression $V - x_3$. This dependence is significantly lower than the dependence on the normal force.

The differential equation contains a constant term which is calculated setting all states to their equilibrium point (0 for all states, $\bar{\omega}$ for $\omega$)

$$0 = T - \frac{r\kappa k_t}{v}\epsilon(\bar{\omega}r - v) \implies \tag{3.36}$$

$$\bar{\omega} = \frac{T + r\kappa K_t\epsilon}{r^2\kappa k_t\epsilon}v. \tag{3.37}$$

Using $x_5 = \omega - \bar{\omega}$ as the new state with equilibrium in zero gives the differential equation

$$\begin{aligned} I_w\dot{x}_5 =& T - \frac{r\kappa k_t}{v}(\epsilon + V - x_3)(x_5 r + \underbrace{\frac{T + r\kappa k_t\epsilon}{r\kappa k_t\epsilon}v - v}_{=:a}) \\ =& -\frac{r\kappa k_t}{v}(\epsilon r x_5 + \underbrace{r x_5 V}_{\approx 0} + aV + -\underbrace{r x_3 x_5}_{\approx 0} - a x_3). \end{aligned} \tag{3.38}$$

As it can be seen two terms are non-linear. Using a first order McLaurin expansion in two variables makes both non-linear terms approximated as zero. Adding

(3.38) to the state space representation in (3.29) gives the linear state space representation

$$\begin{pmatrix} \dot{x}_1 \\ \dot{x}_2 \\ \dot{x}_3 \\ \dot{x}_4 \\ \dot{x}_5 \end{pmatrix} = \begin{pmatrix} 0 & 1 & 0 & 0 & 0 \\ -k_s/m_s & -c_s/m_s & k_s/m_s & c_s/m_s & 0 \\ 0 & 0 & 0 & 1 & 0 \\ k_s/m_u & c_s/m_u & (-k_s - k_t)/m_u & -c_s/m_u & 0 \\ 0 & 0 & \frac{r\kappa k_t a}{vI_w} & 0 & -\frac{r^2 \kappa k_t \epsilon}{vI_w} \end{pmatrix} \begin{pmatrix} x_1 \\ x_2 \\ x_3 \\ x_4 \\ x_5 \end{pmatrix} + \begin{pmatrix} 0 \\ 0 \\ 0 \\ k_t/m_u \\ -\frac{r\kappa k_t a}{vI_w} \end{pmatrix} V \tag{3.39}$$

and the measured output is the zero mean wheel speed $x_5$

$$y = \begin{pmatrix} 0 & 0 & 0 & 0 & 1 \end{pmatrix} \begin{pmatrix} x_1 \\ x_2 \\ x_3 \\ x_4 \\ x_5 \end{pmatrix}. \tag{3.40}$$

The LTI-system (3.39) - (3.40) can, using the notation from (A.3), be represented as a $p \times m$ transfer function $G(s)$ according to

$$G(s) = C(sI - A)^{-1}B + D \tag{3.41}$$

where $p$ is the number of outputs, $m$ is the number of inputs and $s$ is the Laplace operator. For this transfer function, the Laplace description of the system is

$$Y(s) = G(s)U(s). \tag{3.42}$$

Another useful property of a system with the transfer function $G(s)$ is that the relation

$$S_w(i\omega) = |G(i\omega)|^2 S_g(i\omega) \tag{3.43}$$

holds. In this case, $S_g$ is the PSD of the ground (input) and $S_w$ is the PSD of the wheel speeds (output). As this is the frequency response of a system the Laplace operator is $s = i\omega$. This means that given either the road PSD or the wheel speed PSD, the PSD of the other one instantly can be calculated as long as the model transfer function $G(s)$ is of sufficient accuracy for the desired frequencies.

## 3.5 Quarter car parameters

As the road excitation of the vehicle suspension system is unknown, any parameter estimation and other study of the suspensions is heavily limited. A shake test where a compression impulse was sent on the front and rear of the vehicle was

performed. The input impulses are also unknown, but the transients after the impulse are studied as the external input at this point is known to be zero.

The tire spring is neglected as the wheel centre motion is significantly smaller than the vehicle body motion. The differential equation governing the simplified quarter car system is simplified from (3.28a) to

$$m_s\ddot{x}_1 + k_s x_1 + c_s\dot{x}_1 = 0 \tag{3.44}$$

which contains three parameters, but in reality only has to be described by two parameters, the undamped angular frequency $\omega_0 = \sqrt{k/m}$ and the damping ratio $\zeta = \frac{c_s}{2\sqrt{mk}}$ which gives

$$\ddot{x}_1 + \frac{c_s}{m_s}\dot{x}_1 + \frac{k_s}{m_s}x_1 = \tag{3.45}$$

$$= \ddot{x}_1 + 2\zeta\omega_0\dot{x}_1 + \omega_0^2 x_1 = 0. \tag{3.46}$$

These two parameters can possibly be estimated using PEM or other methods. However, even if these parameters are known, the three vehicle parameters will not be known unambiguously without further information.

## 3.6 Combined model

The connection between the suspension/wheel system have been detailed in the previous sections. The slow dynamics and vibration model are also connected as the suspension system and wheels are part of the vehicle model. The forces generated in the contact patch of the wheel and the road heavily controls the vehicle motion. The suspension compression also affects load transfers in the vehicle.

These connection points are $F_x$ and $R_r$ from (3.31) that are the same traction forces as the corresponding signals in (3.11). The complete vehicle model is set-up as quarter car systems in front and back of the one track transient model. These quarter car systems would have different parameter values as the suspension systems in front and rear are very different. The sprung masses would be dependent on the load transfers among the front and rear axes.

# 4

# Results

## 4.1 Quarter car parameters

The study of the suspension system was performed using a shake test where an impulse was sent to the front and rear vehicle body respectively. An accelerometer was placed on the vehicle body just above each axis. The measurement equation is thus

$$y = \ddot{x}_1 = -2\zeta\omega_0 x_2 - \omega_0^2 x_1. \tag{4.1}$$

The results from the parameter estimation using PEM can be seen in Figure 4.1.

The model that is estimated is a underdamped and linear. This does not com-

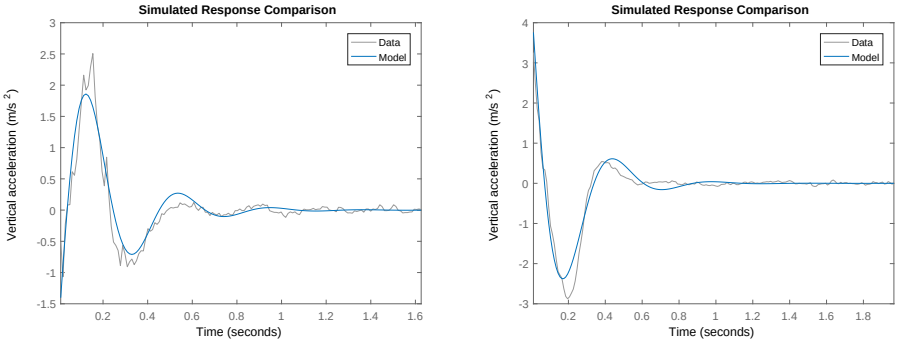


***(a)*** *Front axle.* $\zeta = 0.293$, $\omega_0 = 15.9$ *rad/s.* ***(b)*** *Rear axle.* $\zeta = 0.397$, $\omega_0 = 12.8$ *rad/s.*

***Figure 4.1:*** *Validation data of the damped oscillator quarter car model with parameters estimated using* PEM.

pletely agree with the measured signals. The measured acceleration shows that the frequency tends to increase as the suspended mass velocity is low. The amplitude does also seem to decrease faster for the real system than model. As the model is underdamped, the oscillation will theoretically never die completely. However, a realistic will be overdamped for low velocities due to friction and resistance forces. The damping system is also reasonably designed to be overdamped at low velocities to avoid unnecessary oscillations. This comparison does however show the potential and accuracy of a linear model in regards to the nonlinear system.

## 4.2 Vehicle vibration

The results acquired from the developed vibration methodology are presented in three steps. Firstly, using the road and vehicle models, theoretical wheel speed characteristics are studied. The theoretical description uses typical vehicle and road parameters, as the true parameters are not necessarily known. Secondly, The presented methodology is used to estimate two different road types from collected data. These estimated roads are then used to simulate wheel speed signals, which once again are compared to the measured wheel speed signals.

### 4.2.1 Theoretical PSD

Initially, a theoretical wheel speed PSD is studied and compared to a measured PSD. Using the road descriptions and road parameters in Section 3.3 as $S_g(f)$ inputs in equation (3.43) the theoretical PSD $S_w(f)$ is calculated, see Figure 4.2. The vehicle parameters of a typical passenger vehicle used for the theoretical PSD can be seen in Table 4.1. These vehicle values are the same as the ones used in Türkay and Akcay [21], $I_w$ is a qualified guess while $v$ and $T$ are example values taken from test data.

The theoretical PSD can be compared to the PSD of measured data in Figure 4.3. Note that there is no energy content at frequency zero in the theoretical PSD as the state $x_5$ is equalized around zero. The measured data was taken

***Table 4.1:*** *Model parameters used for calculation of theoretical wheel speed PSD.*

| Parameter | Value |
|---|---|
| $v$ | 14 m/s |
| $m_s$ | 240 kg |
| $m_u$ | 36 kg |
| $c_s$ | 980 Ns/m |
| $k_s$ | 16000 N/m |
| $k_t$ | 160000 N/m |
| $I_w$ | 2 kg m$^2$ |
| $T$ | 20 Nm |

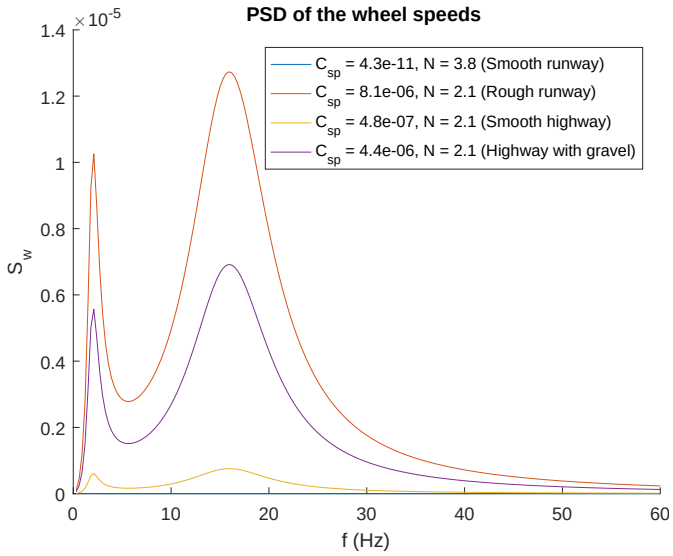


***Figure 4.2:*** *Theoretical PSD of the wheel speeds for various types of roads (road parameters).*

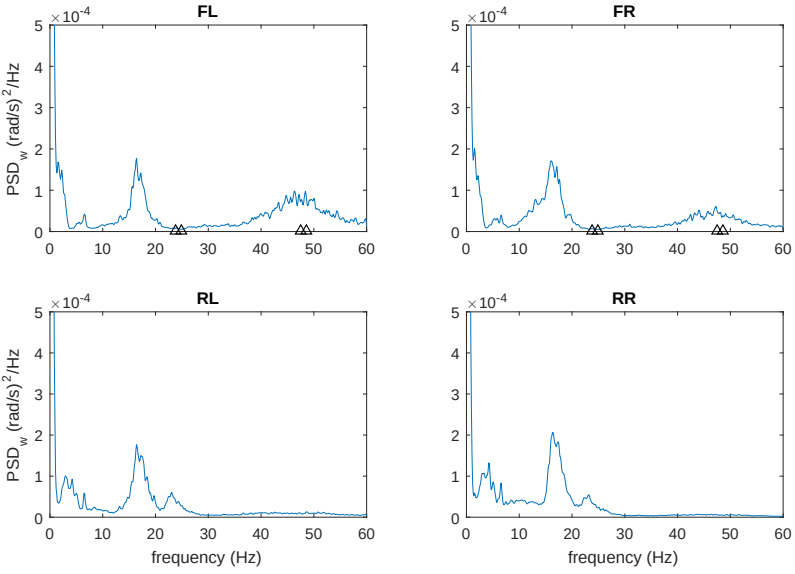


***Figure 4.3:*** *Estimated PSD of the Fiat for a selected section in time. The triangles indicate possible locations of disturbances from the engine.*

from the vehicle travelling at a near constant velocity. The PSD is calculated using

the Matlab function `pwelch` is used to smooth the PSD estimation. The window has been adjusted so that peaks from the wheel suspension and possibly engine disturbances that are known to be there are visible, while other noise is removed.

From the theoretical case a resonance peak is expected below 5 Hz and somewhere between 10 and 20 Hz. The lower peak can be difficult do distinguish from measured data as the vehicle near constant velocity gives a large peak at and around 0 Hz. Apart from that, the higher frequency peak is clearly seen on the non-driving wheels. The exact location and amplitude of this peak does however depend on the vehicle, although, the location usually does not differ too much as long as the vehicle dimensions and suspensions system do not differ considerably.

Apart from other noise and variations, a few small peaks, especially on the driving wheels, can be seen. This is as the driving wheels are subjected to disturbances resulting from the engine and drive-line. According to Johansson [6] an engine with $N$ cylinders and a speed of $\gamma$ RPM resonates the wheel speeds at the frequencies

$$f_{\text{engine}} = \frac{\gamma n}{60 \cdot 2} \tag{4.2}$$

where $n = \{1, 2, \dots\}$ and the main peak is at $n = N$. The possible locations of disturbances of the engine at the frequencies (4.2) are marked by triangles in the figures of PSD of the measured wheel speeds.

The wheel speeds are sampled at 120 Hz, meaning details below the Nyquist frequency 60 Hz can be studied. The effect of the powers in folded frequencies can only be explained and predicted if there is a model of their location, *i.e.* their true frequency is known. This means that it cannot be known if unmodelled disturbances lies within the Nyquist frequency or not. The predicted locations of the engine disturbances have taken this into account.

Some frequency power content can also be seen at 40-50 Hz. This is a result of torsion suspension in the rubber of the tires. This is a tangential/longitudinal force resulting in the tire as the tire is deformed due to longitudinal forces from the engines an and forces in the contact patch [22].

### 4.2.2 Road estimation

Data is collected for two different types of roads: asphalt and gravel. In order for the linearity assumption in the method derivation to hold the vehicle velocity was kept as constant as possible. The data was collected over the same road segment at different velocities to give a wider scope in the data. The PSD of the collected wheels speed signals can be seen in Figure 4.4a. As expected, the vehicle excitations are higher for the gravel road.

Using (3.43), the road is estimated for each of the collected data sets. The estimated road PSD can be seen in Figure 4.4b. Apart from this, the ISO classification road lines are shown as well for comparison.

The main lobe at 17 Hz is the most prominent characteristic that can be seen both in theory and practice. The interval 15-19 Hz of this lobe is marked in Figure 4.4a and its equivalent frequency interval in the spatial domain is marked

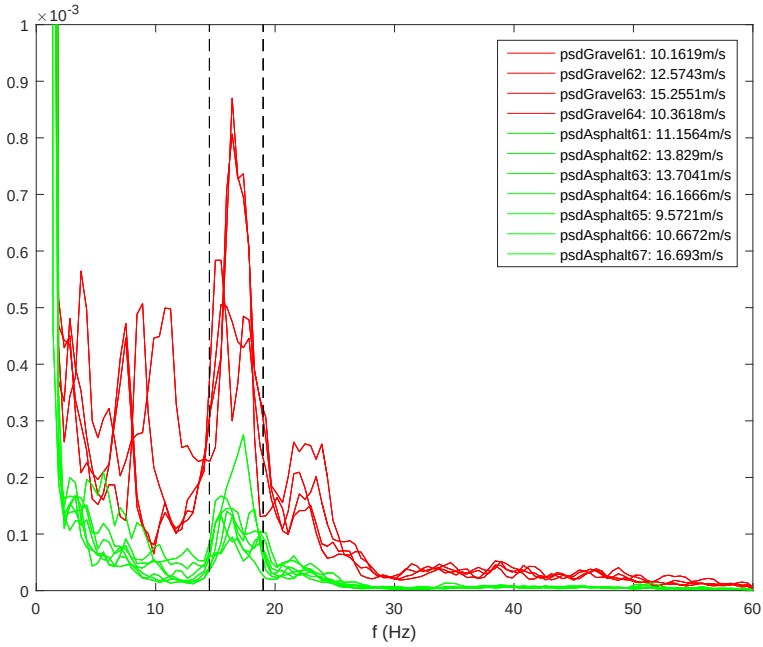


***(a)*** *PSD of the measured wheel speeds.*

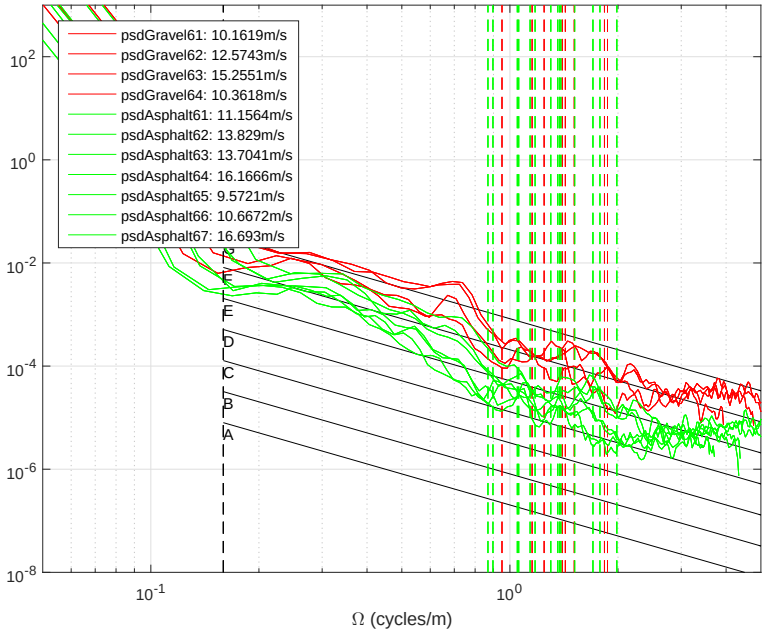


***(b)*** *Estimated road PSD.*

***Figure 4.4:*** *A selected asphalt and gravel road presented in the PSD of the wheel speed and estimated road characteristic at various velocities. The marked frequency intervals are is the main lobe 15-19 Hz in the temporal domain transferred to the linearly equivalent frequencies in the spatial domain for the various test cases.*

in Figure 4.4b. The conversion between the temporal and spatial domain are velocity dependent according to $f = \Omega v$.

### 4.2.3 Wheel speed simulation

From the data in the previous section, an idea of the locations of the road descriptions were given. The two roads are parametrised according on the simplified road description form $S_g(\Omega) = C_{sp}\Omega^{-2}$. The gravel road has the coefficient $C_{sp} = 2.075 \cdot 10^{-4}$ and the asphalt road has $C_{sp} = 5.1 \cdot 10^{-5}$. The data used for the coefficient estimation was solely taken from the marked interval representing the 18 Hz lobe. This is as the model is considered to have highest accuracy in that interval due to good correspondence to the theoretical case. This means that the road model is extrapolated outside of this interval during simulation.

Using this road model description, the wheel speed response to these two types of road is generated. This is performed using white noise with the PSD of the road model as input to the non-linear quarter car model with the wheel dynamics included solved using the solver ode45.

The simulated road can be studied in Figure 4.5 showing the road amplitude in both the time domain and its calculated PSD corrected for the discretisation using the sampling frequency. The simulated wheel speed signals are shown in Figure 4.6 and its calculated PSD is shown. The PSD of the simulated signal in Figure 4.6b is comparable to it measured counterpart in Figure 4.3.

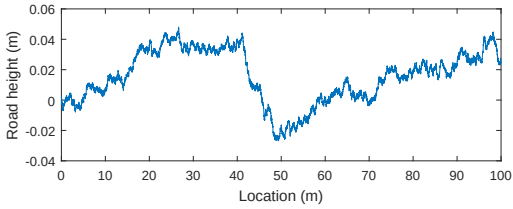


***(a)*** *The road amplitude.*

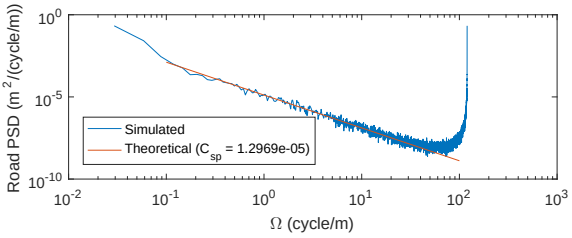


***(b)*** *Spatial PSD of the road amplitude.*

***Figure 4.5:*** *The simulated road and its PSD compared to its theoretical value.*

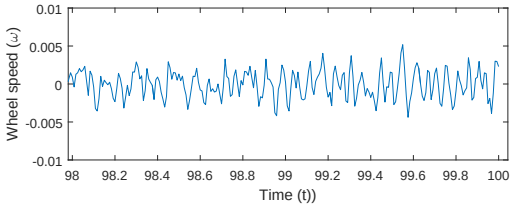


***(a)*** *The wheel angular velocity.*

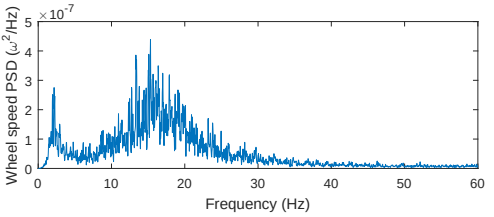


***(b)*** *Temporal PSD of the the wheel angular velocity.*

***Figure 4.6:*** *The simulated wheel speed and its PSD.*

## 4.3 Vehicle motion

The model parameter estimation and validation is performed separately for the longitudinal and transient model.

### 4.3.1 Longitudinal motion

System identification is performed on the problem in (3.8) using PEM. The known inputs are $T_e$, $\eta$ and $R_g$. The velocity $v$ is measured

$$y = v \tag{4.3}$$

which is a known output. The data is collected on a straight road section and PEM is used to estimate the unknown parameters. In order to get a good parameter estimation the dynamics dependent on those parameters must be excited sufficiently. Therefore the data was chosen so that it had a large span in input $T_e$ and in the state $v$ so that the two parameters estimated $\tilde{m}$ and $A_{\text{air}}$ become identifiable. The data was also chosen so that there would be few or no interruptions of bad data where the vehicle was subject to modelled and unknown disturbances.

The simulated response against validation data is shown in Figure 4.7 which has the estimated parameters shown in Table 4.2. It seems clear that the estimated model follows the quick changes in the real system. At a few instances, 600, 800 and 900 seconds, however, the model predict an abrupt drop in the vehicle velocity which did not really occur.

The rolling resistance coefficients $a$ is not estimated as it is a constant term in the differential equation and therefore is not not excited by any input signals or

***Table 4.2:*** *Estimated and measured values.*

| Parameter | Measured/known value | Estimated value | Variance |
|---|---|---|---|
| $\tilde{m}$ (kg) | 1560 (excluding $I_w/r^2$) | 1757 | 1493 |
| $A_{\text{air}}$ (kg/m) | - | 1.21 | 0.00156 |

states. This can be shown by a variable change in the state variable so that the constant term, which is an offset in the state, is removed.

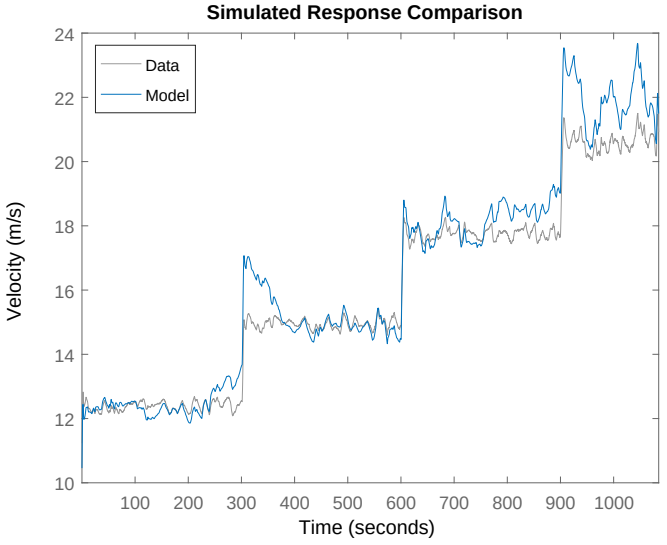


***Figure 4.7:*** *Validation of the longitudinal vehicle motion equation.*

### 4.3.2 Transient motion

System identification is performed on the problem in (3.11) using PEM. Measured signals considered as inputs are $T_e$, $\delta_{sw}$ and $\eta$. Using the wheel speeds the vehicle velocity $v_x$ is known and using the gyroscope the vehicle yaw rate $\Omega_z$ is measured. From this the two measurement equations

$$y = \begin{pmatrix} v_x & \Omega_z \end{pmatrix} \tag{4.4}$$

can be used.

The data was collected during the same restrictions as in the longitudinal case, *i.e.* the data should not be affected by unknown and unmodelled disturbances and the dynamics should be sufficiently excited. One of the terms in the model structure is $l_1 F_{xf} \sin \delta_f$ and it can be seen that for it to be large, the force resulting from the driver input on the road $F_{xf}$ should be large at the same time as the

***Table 4.3:*** *Estimated and measured values.*

| Parameter | Measured/known value | Estimated value | Variance |
|---|---|---|---|
| $\tilde{m}$ (kg) | 1560 (excluding $I_w/r^2$) | 1891 | 237.2 |
| $A_{\text{air}}$ (kg/m) | - | 0.9613 | 0.0003679 |
| $C_{\alpha_f}$ (N) | - | 11960 | 1346000 |
| $C_{\alpha_r}$ (N) | - | 8027 | 420600 |
| $I_z$ (kg m$^2$) | - | 50.0556 | 23976.7 |

vehicle is in a tight curve $\delta_f \gg 0$. This drive style would be considered extreme and this is problematic as this term is difficult to excite in comparison to other terms in the same differential equation. As this term therefore always is relatively small, it becomes much harder to separate the parameters $I_z$, $C_{\alpha_f}$ and $C_{\alpha_r}$ as only the quotients $C_{\alpha_f}/I_z$ and $C_{\alpha_r}/I_z$ become identifiable if $l_1 F_{xf} \sin \delta_f \simeq 0$ which the experiment data shows.

The result of the parameter estimation can be seen in Figure 4.8. Estimated values can be seen in Table 4.3. As in the longitudinal case, the rolling resistance coefficient $a$ is not estimated. It is seen that the cornering stiffness parameters $C_\alpha$ and moment of inertia $I_z$ get unreliable estimations.

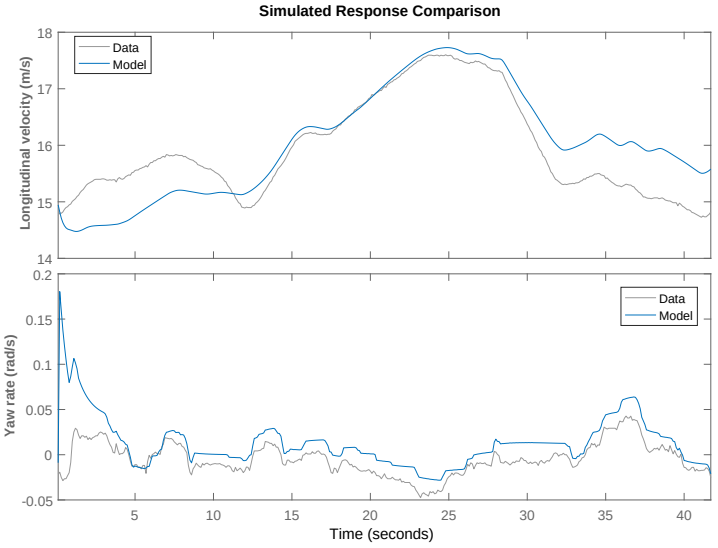


***Figure 4.8:*** *Validation of the transient vehicle motion equations.*

# 5

# Discussion

## 5.1 Presented methodology

The reason the road and wheel/suspension system are separated from the rest of the vehicle dynamics is because a different method of modelling and validation was required for the road model. Given the built-in vehicle sensors, the road as an input signal is unknown. In order to make the road considered known, further tools and sensors are required. Laser scanning could be used to scan an unknown road. However, that information would not be entirely compatible with the simplification of a point contact for the quarter car model used in this thesis. The contact patch is in the order of size 20 centimetres. Data from the laser scanner would be more accurate than that. Using the method proposed in this thesis, the simplification of a 20 centimetre contact patch to a point contact patch makes any model error become fused into the road estimation. A more detailed road description would thus require a more advanced tire model. This could mean numerical solutions, like the use of the finite element method.

Regarding the choice of focusing on the main 18 Hz lobe, this was done as this resonance peak had the most clear agreement of theory and data. Some peaks were explained by other phenomena while others were not. If the interval around 45 Hz would be used for road estimation at those frequencies while not taken into account in the model, it would imprint as a too high road estimate. This is because a higher output power scaled through the model results in a higher input power as the scaling is linear and constant for each vehicle. For the same reason, frequencies at other unexplained peaks were avoided when estimating the road as it is unknown if they are a result of unmodelled dynamics or actual increased road energies at those corresponding frequencies.

There are a few differences in the wheel speeds of the front and rear wheels. The rear wheels have a clearer peak at 3 Hz and an additional peak at 23 Hz

while the front wheels have an additional peak at 45 Hz. The 45 Hz peak is explained by torsional suspension in the tires while the additional rear peaks go unexplained. As the front and rear suspension systems are very different in the vehicle, as, for instance, the suspended mass is much greater in front and the suspension systems have completely different structures, this can give rise to different behaviours and therefore different frequency content in the wheel speeds. Apart from the size and location of a single resonance peak, this is not something that the presented linear quarter car model can explain.

In the transient model, when estimating $I_z$, $C_{\alpha f}$ and $C_{\alpha r}$ separately, the estimation of these parameters is very poor and the low estimate of $I_z$ is clearly unreasonably low. As presented, given that the final term in the differential equation for the yaw rate is relatively small and difficult to excite, these three parameters as a result could become non-identifiable separately. In this case, their quotients would be estimated instead. This means that if the inertia $I_z$ would get measured or estimated elsewhere, proper values of the cornering stiffness coefficients could be deduced as a result.

## 5.2 Future work

One of the main problems encountered was the parameter estimation of the suspension system and wheels. This was, once again, a result of no deterministic knowledge of the road profile. The easiest method of studying these parts would be in a testing rig that can compress the suspension system, *i.e.* the road amplitude would be know. This would also help the study of non-linear sections like the dampers. Improved methods of parameter estimation would be required in order to perform a more thorough validation of the suspension system models and the estimated roads.

The main goal of this thesis was to lay the foundation of a vehicle simulator that could simulate sensor values from various vehicles in different conditions. The main sensors/virtual sensors that were used as outputs as part of the validation process were the vehicle velocity, yaw rate and wheel speeds. There is however a dependence on other information as well that could be regarded as outputs in the simulation model. Sensors could be simulated from the acceleration signals in the models, both a true value of slip can be calculated from its definition using signals in the simulation model as well as simulated sensor values could be used to estimate the slip as a comparison.

The main relation used for the vibration model was the traction force dependence on the normal force. As it can be seen from formulas presented describing the rolling resistance, it is also dependent on the normal force. A future model to be studied could be this dependence with a similar approach as presented in this thesis.

# 6

# Conclusions

A linear model seems sufficient to describe the vertical dynamics to some extent. However, it is difficult to do with realistic parameter values, probably due to the nature of the non-linear dampers. A reasonable explanation is that the linear model becomes a form of combination of the various non-linear suspensions that depend on the different damper sections. Further non-linear damper models are possibly needed in order to fully describe the vehicle behaviour.

The vehicle motion model is validated using estimation and validation data with good accuracy for the most parts. The estimated parameters $m$ and $A_{air}$ are also reasonable and not far of any known values. However, the parameters $I_z$, $C_{\alpha_f}$ and $C_{\alpha_r}$ are very inaccurate. A probable explanation is the loss of identifiability as the system is difficult to excite sufficiently.

At some instances in the slow dynamics validation, the predicted model states deviate greatly from the measured values. The most credible explanation is changes in the wind speeds. This is as the air resistance is the main resistance force and greatly affects the vehicle as it is proportional to the square of the air velocity.

PEM was not possible for the quarter car model as the road is an unknown input. This made the suspension system tightly connected to the road using a vibration model. Its validity is made by a check of credibility using road profile estimation in the frequency domain. The estimated asphalt and gravel roads are reasonable, at least in the frequency intervals that predict the clearest peaks. Using the extrapolated road model the wheel speeds can be simulated. These simulated wheel speeds characteristics are in agreement with theory. The main lobe at 20 Hz is also in agreement with measured data.

The imposed limitation of tools and sensors available in this thesis greatly affected the potential of accurate parameter estimation of the developed models. By extension, this also affects proper validation of the vibration model. The

slow dynamics model was restricted to just a few states and a few parameters. Several parameters were not identifiable or separable. In order to accurately estimate the parameters, especially if the model complexity is increased, additional tools and measurement equations are needed. Alternatively, tests must be performed during more controlled scenarios. For instance, it was seen how greatly the wind speed affected the longitudinal estimation. Either testing in an environment without wind disturbances or additional wind speed measurements could increase the model accuracy in this regard.

# Appendix

# A

# State space models

A common model structure is the state space model. Its non-linear form is

$$\dot{x} = f(x, u) \tag{A.1a}$$

$$y = h(x, u) \tag{A.1b}$$

where $x$ is the system state, $u$ is the input signal, $y$ is the measured output and $f$ and $h$ are non-linear functions. While many physical systems are non-linear by their nature, they can often be considered linear around a certain linearisation point. In a two variable function the first order Taylor expansion gives

$$f(x, y) \approx f(a, b) + \left.\frac{\partial f(x, y)}{\partial x}\right|_{a,b} (x - a) + \left.\frac{\partial f(x, y)}{\partial y}\right|_{a,b} (y - b) \tag{A.2}$$

which is a linearisation in a continuous and differentiable linearisation point $(a, b)$.

The linear state space structure is

$$\dot{x} = Ax + Bu \tag{A.3a}$$

$$y = Cx + Du \tag{A.3b}$$

for the matrices $A$, $B$, $C$ and $D$. The model structure in (A.1) and (A.3) are usually given by knowledge of the physical system where the desired properties often are described using regular physical relationships.

# Bibliography


[1] R. Wade Allen and Theodore J. Rosenthal. Requirements for vehicle dynamics simulation models. *SAE*, 1994. Cited on page 2.

[2] Tobias Hammarling. Estimation of lateral friction and tire-road forces, based on automotive grade sensors. Master's thesis, Linköping university, 2015. Cited on page 16.

[3] Reyhaneh Hesami and Kerry J. McManus. Signal processing approach to road roughness analysis and measurement. *IEEE*, 2009. Cited on page 3.

[4] Carsten Hoever and Wolfgang Kropp. A model for investigating the influence of road surface texture and tyre tread pattern on rolling resistance. *Science direct*, 2015. Cited on page 2.

[5] Cao Dong Jiang, Lin Cheng, Sun Fengchun, and Chang Hongjie. Simulation of road roughness based on using ifft method. *IEEE*, 2013. Cited on page 3.

[6] Robert Johansson. Modeling of engine and driveline related disturbances on the wheel speed in passenger cars. Master's thesis, Linköping university, 2012. Cited on page 28.

[7] Rune Karlsson, Ulf Hammarström, Harry Sörensen, and Olle Eriksson. Road surface influence on rolling resistance. *VTI publications*, 2011. Cited on page 3.

[8] Sujay J. Kawale and John B. Ferris. Developing a methodology to synthesize terrain profiles and evaluate their statistical properties. *SAE*, 2011. Cited on page 4.

[9] Jacob N. Lambeth, John Ferris, Alexander Reid, and David Gorsich. Developing a compact continuous-state markov chain for terrain road profiles. *SAE*, 2013. Cited on page 4.

[10] Bin Li, Xiaobo Yang, and James Yang. Tire model application and parameter identification-a literature review. *SAE*, 2014. Cited on page 4.

[11] L. Li and C. Sandu. Stochastic analysis of tire - force equations. *SAE*, 2007. Cited on page 4.

[12] Lennart Ljung and Torkel Glad. *Modellbygge och simulering*. Studentlitteratur, second edition, 2004. Cited on pages 4 and 9.

[13] Mikael Olofsson. *Signal theory*. Studentlitteratur, 1:1 edition, 2011. Cited on page 9.

[14] Hans B. Pacejka. *Tyre and vehicle dynamics*. Elsevier Ltd., second edition, 2006. Cited on page 4.

[15] Wei Quan, Hua Wang, Chaoyi Wang, and Xiangchen Hou. Evaluation of road roughness based on multi-fractal theory. *IEEE*, 2013. Cited on page 3.

[16] J. J. Rath, K. C. Veluvolu, and M. Defoort. Simultaneous estimation of road profile and tire road friction for automotive vehicle. *IEEE*, 2015. Cited on pages 2 and 3.

[17] Ferhat Saglam and Y. Samim Unlusor. Identification of low order vehicle handling models from multibody vehicle dynamics models. *IEEE*, 2011. Cited on page 2.

[18] C. Sandu, A. Sandu, and L. Li. Stochastic modeling of terrain profiles and soil parameters. *SAE*, 2005. Cited on page 3.

[19] M. A. Soliman. Effect of road roughness on the vehicle ride comfort and rolling resistance. *SAE*, 2006. Cited on page 2.

[20] Bangalore A. Suresh and Brian J. Gilmore. Vehicle model complexity how much is too much. *SAE*, 1994. Cited on page 4.

[21] Semiha Türkay and Hüseyin Akcay. A study of random vibration characteristics of the quarter-car model. *Science direct*, 2004. Cited on pages 3, 17, and 26.

[22] Takaji Umeno, Katsuhiro Asano, Hideki Ohashi, Masahiro Yonetani, Toshiharu Naitou, and Takeysau Taguchi. Observer based estimation of parameter variations and its application to tyre pressure diagnosis. *Science Direct*, 2001. Cited on page 28.

[23] Gabriele Vandi, Davide Moro, and Fabrizio Ponti. Vehicle dynamics modeling for real-time simulation. *SAE*, 2013. Cited on page 2.

[24] Shifeng Wang, Sarath Kodagoda, and Rami Khushaba. Towards speed-independent road-type classification. *IEEE*, 2012. Cited on page 3.

[25] J. Y. Wong. *Theory of ground vehicles*. John Wiley & sons, inc., fourth edition, 2008. Cited on pages 2, 13, 14, and 16.

[26] Hiroshi Yokohama and Robert B. Randall. Investigation of road surface roughness effect on tread rubber friction with fea. *SEA*, 2009. Cited on page 4.